© MAR 2026 | IRE Journals | Volume 9 Issue 9 | ISSN: 2456-8880
DOI: https://doi.org/10.64388/IREV9I9-1715554

Comparison of The Strength of Eej from Geomagnetic Data at Addis Ababa and Mbour for 27th January, 27TH February, 27th March 2013

EKWUBIRI, E.C.
Department of Physics, University of Benin, Benin City

Abstract- ***The INTERMAGNET Database was used to evaluate a detailed analysis of ground-based geomagnetic measurements from Addis Ababa (lat. 9.000 N, long. 38.800 E) and Mbour (lat. 14.390 N, long. 16.900 W) in the Africa/Indian Ocean region. Using the available dataset, the study period was chosen so that the data interval used was for the entire day (24 hours) of January 27, February 27, and March 27, 2013. The dataset utilized was for fluctuations in disturbed hours, and the average values of the per-minute data obtained from the INTERMAGNET Station were translated to per-hour readings. Using the average value of all the datasets examined for each geomagnetic component, the strength of the Equatorial Electrojet (EEJ) was calculated. A visualization of the geomagnetic H&X components across time showed how variable the EEJ was per minute. The daily average of the data revealed that the EEJ strength for the Horizontal component of the Earth's Magnetic field (H-component) at Addis Ababa Station on January 27, February 27, and March 27, 2013, was 36177.11nT, 36247.43nT, and 36201.30nT, respectively while the EEJ strength for X-component at Mbour station on January 27, February 27, and March 27, 2013, was 32121.04nT, 32160.54nT, and 32161.63nT. The results obtained for Addis Ababa and Mbour show the equatorial Electrojet (EEJ) strength is supplementary at Addis Ababa than at Mbour on the same days.***

Index Terms- ***Equatorial Electrojet, Plasma, Geomagnetic Field, Intermagnet, and Ionosphere***

I. INTRODUCTION

Probes of the atmosphere, particularly the ionosphere, the region that contains large amounts of protons and ions that form a plasma with varying densities at different layers, are necessary to compare the strength of the equatorial electroject (EEJ) from geomagnetic data at the Addis Ababa and Mbour stations. The geomagnetic field will be thoroughly discussed in this paper as a factor that influences the ionosphere's EEJ intensity (Ekwubiri & Aiyohuyin, 2026). Data from the observatories in Addis Ababa and Mbour were chosen and processed to produce the appropriate data for comparing the equatorial electrojet's strength. Free electrons are found in the ionosphere, the region of the upper atmosphere where they are dense enough to significantly affect how radio frequency waves travel. The sun and its activities are the main cause of ionization in this area. Geographical location (polar auroral zones, mid-attitude, and equatorial region), time (sunspot cycle, seasonally, and diurnally), and specific solar-related ionospheric disturbances result in significant variations in ionosphere structure and peak densities (Ratcliffe, 1972). The sun's X-ray, UV, and corpuscular (collection) radiation are responsible for the majority of the ionization.

The Earth's rotation with respect to the sun produces the most obvious effect. In the bright atmosphere, ionization rises, while in the shaded environment, it falls. Cosmic rays contribute very little to ionization, despite the sun being the main source. The distribution of the ionization is impacted by any disturbance in the atmosphere. Similar to the solar terrestrial environment, plasma makes up a significant portion of the ionosphere. Its electron and ion densities are roughly equal, and its dynamics are influenced by both local and distant factors (Hargreaves, 1992). Numerous factors, such as the atmosphere's acoustic movements, electron magnetic emissions, and variations in the geomagnetic field, regulate the dynamic ionosphere. The ionosphere serves as a platform for monitoring atmospheric events because of its high sensitivity to changes in the atmosphere. There is convincing evidence of an ionospheric precursor to major earthquakes that can be utilized as a prediction in certain cycles. In

© MAR 2026 | IRE Journals | Volume 9 Issue 9 | ISSN: 2456-8880
DOI: https://doi.org/10.64388/IREV9I9-1715554

addition to the evident acoustic waves produced by electromagnetic emission (EMEs) prior to and during an earthquake, EMEs have been found in the ionosphere as early as six days prior to a major earthquake (Jursa, 1985). Because it is ionized by solar radiation, the ionosphere, which is a component of the upper atmosphere and ranges in altitude from roughly 85 km to 600 km, is made up of parts of the mesosphere, thermosphere, and exosphere. It creates the inner edge of the magnetosphere and has a significant role in electricity. It is useful because it affects radio transmission to far-off locations on Earth, among other things (Forbes, 1981). Encircling the Earth from a height of roughly 50 km to over 1000 km is a shell of electrons and electrically charged atoms and molecules known as the ionosphere. Its existence is mostly due to the Sun's UV radiation. The troposphere is the lowest layer of the Earth's atmosphere, extending from the surface to a distance of roughly 10 kilometers (6.2 miles). Above 10 km, the stratosphere is followed by the mesosphere. The ozone layer is formed in the stratosphere by incoming solar energy. The thermosphere's atmosphere is so thin at altitudes more than 80 km (50 mi) that free electrons can live there for brief periods before being captured by a neighboring positive ion. There are enough of these free electrons to have an impact on radio transmission. The term "ionosphere" refers to this area of the atmosphere that is ionized and includes plasmas. The electromagnetic force in plasma attracts the positive ions and the negative free electrons, but they are too energetic to remain fixed together in an electrically neutral molecule (Kelly, 1989).

II. THEORETICAL BACKGROUND

2.1.1 Current System In The Equatorial Region

The two main types of atmospheric composition are neutral gas, which is made up of neutral atoms and molecules, and ionospheric plasma, which is made up of free ions and free electrons produced by particle dissociation, precipitation at high latitudes, and energetic ultraviolet (EUV) solar radiation at all latitudes (Fejer, 2010). The intensity of the ionizing radiation and the density of the neutral gas determine how quickly ions are produced with height (Campbell, 1990).

2.1.2 Conductivity in the Absence of a Magnetic Field

When discussing electrical conductivity in the ionosphere, let's start with the scenario in which an electric field is present but the magnetic field is not. In this scenario, the individual gas particles move at their thermal velocity as a result of collisions, which are accelerated in the electric field by the equation: (Kivelson and Russell, 1995).

$$a = q\frac{E}{m} \qquad (2.1)$$

To determine the charged particle's mean velocity vector, we suppose that the particle loses the extra velocity it gained in the electric field in each collision at the moment, but that it gains an additional velocity following the first and second collisions, which is expressed as:

$$v(\tau_1) = a(\tau_1) \qquad (2.2)$$

The average velocity in time interval is shown in the formula given as (Ekwubiri and Said, 2015):

$$\bar{v}_1 = \frac{1}{\tau_1}\int_0^{\tau_1} a t dt = \frac{1}{2} a\tau_1 \qquad (2.3)$$

Similarly,

$$\bar{v}_2 = \frac{1}{2} a\tau_2 \qquad (2.4)$$

But the average time interval duration is:

$$\bar{\tau} = \left[\frac{\tau_1 + \tau_2}{2}\right] \qquad (2.5)$$

The average velocity for the two intervals will now become:

$$\bar{v}_{1,2} = \frac{\tau_1\bar{v}_1 + \tau_2\bar{v}_2}{\tau_1 + \tau_2}$$

$$= 1/2\,\frac{\tau_1}{\bar{\tau}}\bar{v}_1 + 1/2\,\frac{\tau_2}{\bar{\tau}}\bar{v}_2 \qquad (2.6)$$

© MAR 2026 | IRE Journals | Volume 9 Issue 9 | ISSN: 2456-8880
DOI: https://doi.org/10.64388/IREV9I9-1715554

Where $\{\rho(\tau_1) = 1/2 \frac{\tau_1}{\bar{\tau}} \bar{v}_1 \text{ and } \rho(\tau_2) = 1/2 \frac{\tau_2}{\tau} \bar{v}_2\} = \rho(\tau) =$ is the realistic assumption on the probability distribution of time intervals between two collisions with respect to the length (L). We can now take mean velocity as: $\bar{v} = \int_0^\infty \rho(\tau) \frac{\tau}{\bar{\tau}} \frac{1}{2} a\tau d\tau$

$$= \frac{a}{2\bar{\tau}} \int_0^\infty \tau^2 \rho(\tau) d\tau \qquad (2.7)$$

Assuming that $v_E \ll v_{thermal}$ according to radioactive decay, where the time of the subsequent decay does not exclusively depend on the time of the erstwhile decay, then we assume an exponential probability distribution as:

$$\rho(\tau) = \frac{1}{\bar{\tau}} \left[exp \frac{-\tau}{\bar{\tau}}\right] \qquad (2.8)$$

Collision less time intermission will mean:

$$E(\tau) = \int_0^\infty \tau \, \rho(\tau) d\tau = \bar{\tau} \qquad (2.9)$$

From equation (2.7), we can write:

$$\bar{v} = \frac{a}{2\bar{\tau}} \int_0^\infty \tau^2 \frac{1}{\bar{\tau}} [\exp \frac{-\tau}{\bar{\tau}}] \, d\tau$$

$$= \frac{a}{2\bar{\tau}} 2\bar{\tau}^2$$

$$= a\bar{\tau} \qquad (2.10)$$

When we Substitute equation (2.1) into equation (2.10) we obtain:

$$\bar{v} = q \frac{E}{m} \bar{\tau} \qquad (2.11)$$

Equation (2.11) is the mean velocity of a particular particle in the nonappearance of a magnetic field. To estimate the contemporary density vector (j) of the mean velocity for completely charged particles through ion density number and electron density number, we can write that:

$$j = n_i \bar{v}_i q_i + n_e \bar{v}_e q_e$$

$$= ne^2 \left[\frac{\bar{\tau}_i}{m_i} + \frac{\bar{\tau}_e}{m_e}\right] E \qquad (2.12)$$

Given that, $\bar{\tau} = \frac{1}{v}$, substitute it into equation (2.12) to obtain:

$$j = ne^2 \left[\frac{1}{m_i V_i} + \frac{1}{m_e V_e}\right] E \qquad (2.13)$$

But $\sigma_0 = ne^2 \left[\frac{1}{m_i V_i} + \frac{1}{m_e V_e}\right]$

$$\therefore j = \sigma_0 E \qquad (2.14)$$

The current density vector of a specific type of charged particle is equal to the conductivity of its free space, as demonstrated by equation (2.14).

2.1.3 Conductivity in the Presence of a Magnetic Field

At this juncture, it is indispensable to fragment the electric field into components: E_p corresponding to the magnetic field and E⊥ vertical to the magnetic field (Campbell, 1989).

2.1.4 Conductivity Parallel to Magnetic Field

Subsequently, Lorentz forces do not act on a particle moving in the parallel direction to the magnetic field, we may write that:

$$j_\parallel = \sigma_0 E_\parallel$$

Such that σ_0 is also called parallel conductivity.

2.1.5 Conductivity Perpendicular to the Magnetic Field

At this point, the charged particle acceleration is being predisposed by two contributors written as:

$$a = q \frac{E_\perp}{m} + \frac{q}{m}(v \times B) \qquad (2.16)$$

Where this equation $\frac{q}{m}(v \times B)$ *is* Lorentz acceleration, *and* $q \frac{E_\perp}{m}$ is a perpendicular field effect.

Considering three coordinate systems concerning unit vectors, we have:

© MAR 2026 | IRE Journals | Volume 9 Issue 9 | ISSN: 2456-8880
DOI: https://doi.org/10.64388/IREV9I9-1715554

$$\hat{X} = \frac{\vec{E}_\perp}{|\vec{E}_\perp|} \; ; \; \hat{Y} = -\frac{\vec{v} \times \vec{B}}{|\vec{v} \times \vec{B}|} \; ; \; \hat{Z} = \frac{\vec{B}}{|\vec{B}|} \quad (2.17)$$

Since our concentration is the particle movement in the (x, y) plane, we can write that:

$$a_y = \frac{q}{m}E_\perp + \frac{q}{m}(v_y B) \quad (2.18)$$

$$a_x = -\frac{q}{m}(v_x B) \quad (2.19)$$

Where $\vec{E}_\perp = |\vec{E}_\perp| \; and \; \vec{B} = |\vec{B}|$

Then,

$$\omega = \frac{q}{m}B \quad (2.20)$$

Gyro frequency $(|\omega|)$ is always positive, while ω carries the sign of the charge (q) (Alex and Mukherjee, 2001). Considering the above equation, we can further define another expression using the below equation as expressed from the gyro frequency formula;

$$a_\perp = \frac{q}{m}E_\perp \quad (2.21)$$

Formerly, equation (2.18) and (2.19) can be written as:

$$a_y = a_\perp + \omega v_y \quad (2.22)$$

$$a_x = -\omega v_x \quad (2.23)$$

Subsequently, acceleration is a temporal derivation of velocity, we can then write that:

$$\dot{v}_y = a_\perp + \omega v_y \quad (2.24)$$

$$\dot{v}_x = -\omega v_x \quad (2.25)$$

Captivating the second differential derivative of equations (2.24) and (2.25), we obtain:

$$\ddot{v}_x = -\omega^2 v_x \rightarrow \ddot{v}_x = C\sin(\omega t + \phi) \quad (2.26)$$

$$\ddot{v}_y = \frac{v_y - a_\perp}{\omega} \rightarrow \ddot{v}_y = C\cos(\omega t + \phi) - \frac{a_\perp}{\omega} \quad (2.27)$$

We can harmonize equations (2.24 and 2.25) by considering the Constants C and Ø which are the initial velocity of the particle under investigation after collision.

Using $v = \acute{v} + v_0$ and substitute into equation (2.16), the initial velocity (v_0) will result in the additional gyration, which will cancel out all collisions, thereby giving the need to set

$V_x(0) = 0 \; and \; V_y(0) = 0, to \; obtain \; \phi = 0 \; and, C = \frac{a_\perp}{\omega}$. Then, the particle Trajectories results as:

$$\ddot{v}_x = \frac{a_\perp}{\omega}(\sin \omega t) \quad (2.28)$$

$$\ddot{v}_y = \frac{a_\perp}{\omega}(\cos \omega t - 1) \quad (2.29)$$

The average velocity for a solitary time interval between two collisions will now give:

$$\bar{v}_x(\tau) = \frac{1}{\tau}\int_0^\tau v_x(t)dt \quad (2.30)$$

$$= \frac{a_\perp}{\tau\omega}\int_0^\tau \sin \omega t \, dt \quad (2.31)$$

$$= \frac{a_\perp}{\tau\omega^2}(1 - \cos \omega\tau) \quad (2.32)$$

Conjoining the average mean velocity over the entire possible collision-less intervals and the probability distribution $\rho(\tau)$ gives rise to:

$$\bar{v}_x = \int_0^\infty \rho(\tau)\frac{\tau}{\bar{\tau}}v_x(\tau)d\tau \quad (2.33)$$

$$\frac{1}{\bar{\tau}}\int_0^\infty \rho(\tau)\frac{a_\perp}{\omega^2}(1 - \cos\omega\tau)d\tau \quad (2.34)$$

$$= \frac{a_\perp}{\tau\omega^2}\left(\int_0^\infty \rho(\tau)d\tau - \int_0^\infty \rho(\tau)\cos\omega\tau d\tau\right) \quad (2.35)$$

$$= \frac{a_\perp}{\tau\omega^2}\left(1 - \frac{\bar{\tau}}{\bar{\tau}^2 + \omega^2}\right) \quad (2.36)$$

$$= \frac{a_{\perp\bar{\tau}}}{\bar{\tau}^2 + \omega^2} \quad (2.37)$$

Recall that: $\bar{\tau} = \frac{1}{\nu} \; and \; a_\perp = q\frac{E_\perp}{m}$ (2.38)

© MAR 2026 | IRE Journals | Volume 9 Issue 9 | ISSN: 2456-8880
DOI: https://doi.org/10.64388/IREV9I9-1715554

Substitute equation (2.38) into equation (2.37) to obtain:

$$\bar{v}_x = \frac{q\,V}{m(v^2+\omega^2)}E_\perp \quad (2.39)$$

To compute the current density commencing from mean particle velocity, we write:

$$j_x = n\left(\bar{v}_{x,i}q_i \times \bar{v}_{x,e}q_e\right) \quad (2.40)$$

$$= ne^2\left[\frac{v_i}{m_i(v_i^2+\omega_i^2)} + \frac{v_e}{m_e(v_e^2+W\omega_e^2)}\right]E_\perp \quad (2.41)$$

Where

$$\sigma p = ne^2\left[\frac{v_i}{m_i(v_i^2+\omega_i^2)} + \frac{v_e}{m_e(v_e^2+W\omega_e^2)}\right]E_\perp$$

Equation 2.41 becomes;

$$j_x = \sigma p \quad (2.42)$$

According to Jursa (1985), equation (2.42) demonstrates that the current density derived from the mean particle velocity is equivalent to the Pederson conductivity parallel to the electric field component perpendicular to the magnetic field. Similarly, we first write the mean velocity particle in the y direction as follows to get the conductivity perpendicular to the magnetic field (B) and perpendicular to the electric field $E^{\perp}$:

$$\bar{v}_y = \frac{q}{m}\left(\frac{-\omega}{v^2+\omega^2}\right)E_\perp \quad (2.43)$$

Considering;

$$q_i = e \text{ while } q_e = -e, \text{since } \omega = \frac{q}{m}B$$

The gyro-frequency of ions will be given as:

$$\omega_{g,i} = |\omega_i| = \omega_i \quad (2.44)$$

While the gyro-frequency of electrons is:

$$W_{g,e} = |w_e| = w_e \quad (2.45)$$

Therefore,

$$j_y = n\left(\bar{v}_{y,i}q_i + \bar{v}_{y,e}q_e\right) \quad (2.46)$$

$$= n_e^2\left[\frac{-\omega_i}{m_i(v_i^2+\omega_i^2)} + \frac{-\omega_e}{m_e(v_e^2+\omega_e^2)}\right]E_\perp \quad (2.47)$$

$$= n_e^2\left[\frac{-\omega_i}{m_i(v_i^2+\omega_i^2)} + \frac{|\omega_e|}{m_e(v_e^2+\omega_e^2)}\right]E_\perp \quad (2.48)$$

$$= n_e^2\left[\frac{|\omega_e|}{m_e(v_e^2+\omega_e^2)} - \frac{\omega_i}{m_i(\omega_i^2+\omega_i^2)}\right]E_\perp \quad (2.49)$$

Where

$$\sigma H = n_e^2\left[\frac{|\omega_e|}{m_e(v_e^2+\omega_e^2)} - \frac{\omega_i}{m_i(\omega_i^2+\omega_i^2)}\right]E_\perp$$

Then equation (2.49) becomes;

$$j_x = \sigma H \quad (2.50)$$

The current density from the gyro-frequency of ions and electrons is equal to the hall conductivity, as demonstrated by equation (2.50). Keep in mind that the eastward movement of the solar wind plus the effects of Pederson and Hall conductivity at +3 degrees equator result in a current augmentation known as the Equatorial electrojet (Briggs, 1984).

2.1.6 Conductivity and Altitude

As the conductivity increases parallel to the magnetic field, there are fewer collisions with the neutral gas. Vertical conductivity is always higher than conductivity perpendicular to the magnetic field. At high altitudes, the ionosphere exhibits such strong parallel conductivity that the magnetic field lines can be considered the equipotential of the electric field (Campbell, 1990). The ratio of the collision frequency to the gyro frequency determines the velocity of a particular kind of charged particle perpendicular to the magnetic fields. (ω_g). Pedersen current is created when the collision frequency is higher than the gyro frequency ($v > \omega_g$), since the collision stops the particles from gyrating and causes them to move in the direction of the electric field; conversely if the gyro frequency is higher than the collision frequency($\omega_g > v$), the particles primarily drift perpendicular to the electric field (Kelly, 1989). The electrical characteristics of the ionosphere change significantly with altitude due to variations in the behavior of ions and electrons. While ions continue to travel in the direction of the

electric field, electrons begin to gyrate and drift perpendicular to it at elevations more than 70 km. Hall conductivity is the outcome of these variations. At this point, a neutral wind carries the ions with it, and the electrons collide with the neutral gas considerably more frequently while they are still gyrating. They also instantly change direction without being affected by the solar wind, resulting in a charge separation that resembles a dynamo. When the ions and electrons drift in the same direction, there is no electric current, which causes the hall conductivity to drop dramatically. At elevations higher than 130 km, the ions gyrate and drift perpendicular to the magnetic field (Alex and Mukherjee, 2001).

2.1.7 Equatorial electrojet and cowling conductivity

The right-handed geomagnetic coordinate system, where x points north, y points east, and z points down, can be used to explain the high electrical current (E_y) that is often conducted eastward at the magnetic equator during the day. A hall current produced by an initial eastward electric field (E_y) is expressed as follows:

$$j_z = \sigma_H E_y \quad (2.51)$$

This results in a negative charge on the top side of the E-region and a positive polarization charge on the bottom side. This process, which continues until the electrostatic secondary polarization field stops the vertical hall current, results in the following equations.

$$\text{I} j_y = \sigma_p E_y - \sigma_H E_z \quad (2.52)$$

$$\text{II } j_z = \sigma_p E_z + \sigma_H E_y \quad (2.53)$$

$$j_z - \sigma_p E_z = \sigma_H E_y$$

$$\sigma_p E_z = j_z - \sigma_H E_y$$

$$E_z = \frac{j_z}{\sigma_p} - \frac{\sigma_H}{\sigma_p} E_y \quad (2.54)$$

But, if $j_z = 0$, then equation (2.59) becomes;

$$E_z = -\frac{\sigma_H}{\sigma_p} E_y \quad (2.55)$$

From equation (2.57), we can substitute equation (2.60) into it, to obtain

$$j_y = \sigma_p E_y - \sigma_H \left(-\frac{\sigma_H}{\sigma_p} E_y\right) \quad (2.56)$$

$$= \sigma_p E_y + \sigma_H \left(\frac{\sigma_H}{\sigma_p} E_y\right)$$

$$= \sigma_p \left(1 + \frac{\sigma_H^2}{\sigma_p^2}\right) E_y \quad (2.57)$$

$$\therefore \quad j_y = \sigma_C E_y \quad (2.58)$$

Where

$$\sigma_C = \sigma_p \left(1 + \frac{\sigma_H^2}{\sigma_p^2}\right) = cowling\ conductivity$$

III. MATERIALS AND METHODS

Using data from the INTERMAGNET database, the strength of EEJ in the ionosphere was estimated using data from ground-based magnetometers at the Addis Ababa and Mbour observatories. Ottawa GIN translated the original data file from INTERMAGNET Imfv1.22 data that was obtained from the magnetometer. These records were taken from a data file that was reported. Owing to their size, the INTERMAGENT database compressed these data files for convenient transport. To convert these data files into a readable format, software known as WinRAR was utilized. These records were made in minutes, which were then converted to readings in hours by averaging the minutes. The resulting tabulation was used to create graphs for the Addis Ababa and Mbour stations for the 27th January, 27th February, and 27th March 2013 periods, respectively. The daily values of the geomagnetic component (XYZF) for averaged Cartesian coordinates and (HDZF) for magnetometer calibrations are displayed in Tables 3.1 and 3.2 respectively.

© MAR 2026 | IRE Journals | Volume 9 Issue 9 | ISSN: 2456-8880
DOI: https://doi.org/10.64388/IREV9I9-1715554

Table 3.1: Averaged Daily Data for Addis Ababa in Nanotesla (nT)

DATE	TIME	AAEH	AAED	AAEZ	AAEF
27/01/13	00.00 - 23.59	36177.11	1186.57	1840.99	36261.54
27/02/13	00.00 – 23.59	36247.43	1188.47	1849.02	36310.83
27/03/13	00.00 – 23.59	36201.30	1179.66	1860.85	36264.60

Table 3.2: Averaged Daily Data for Mbour in Nanotesla (nT)

DATE	TIME	MBOX	MBOY	MBOZ	MBOF
27/01/13	00.00 – 23.59	32121.04	-4335.68	4233.589	32688.02
27/02/13	00.00 – 23.59	32160.54	-4343.47	4217.81	32725.60
27/03/13	00.00- 23.59	32161.63	-4328.47	4224.303	32726.02

3.1 Comparisons of EEJ at Addis Abba and Mbour

This effect is approached graphically as shown below;

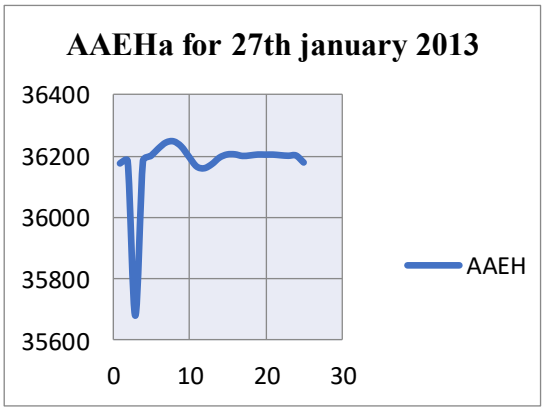

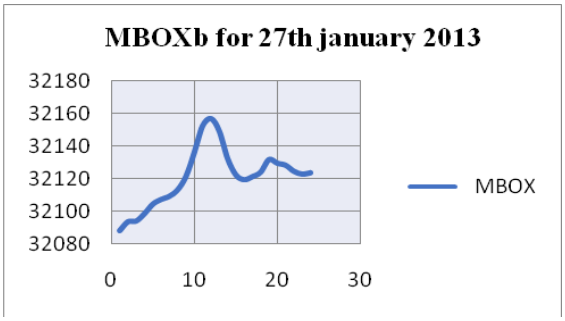

Fig 3.1a&b: Geomagnetic H&X-component against time (UT)

Figure 3.1a shows a dramatic decrease in EEJ intensity during the hour of 0200 UT, followed by a sharp increase in EEJ intensity with a constant strength for the remaining hours of January 27, 2013. The strength of EEJ in Fig. 3.1b, on the other hand, began to climb at 0100UT, peaked at 1100UT, and then abruptly decreased at 1300UT before slightly increasing and retarding once again. This indicates that on January 27, 2013, the equatorial electrojet (EEJ) strength at Addis Ababa experienced a sharp decline and then a sharp increase before remaining somewhat stable. In contrast, the EEJ strength at Mbour was unstable, fluctuating between a sharp decline and a slight increase before ending.

© MAR 2026 | IRE Journals | Volume 9 Issue 9 | ISSN: 2456-8880
DOI: https://doi.org/10.64388/IREV9I9-1715554

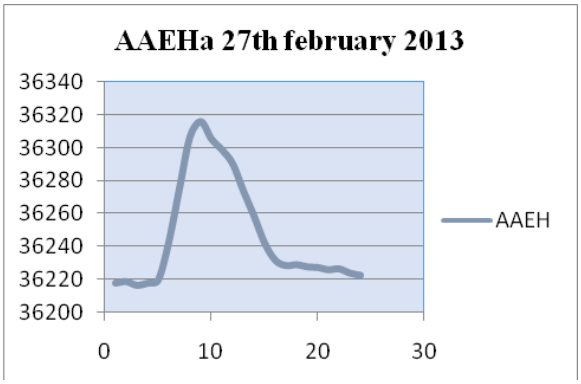

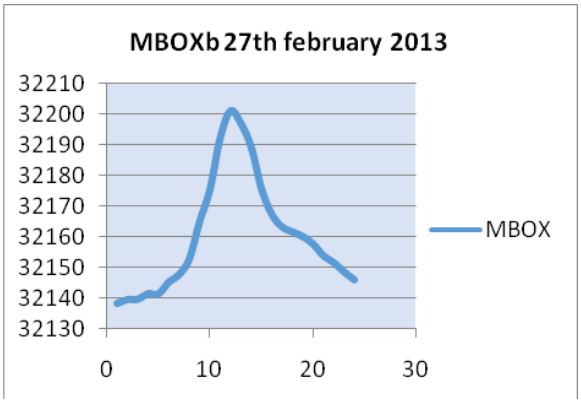

Fig 3.2a&b: Geomagnetic H&X-component against time (UT)

The EEJ strength is affected in the same way as Figs. 3.2a and 3.2b; however, Fig. 3.2a's peak time is at 0900 UT, while Fig. 3.2b's is at 1200 UT. Figure 3.2a shows a sharper increase and drop in EEJ strength than Figure 3.2b. The geometry of the two graphs in Figure 3.2a and 3.2b is the same but slightly opposite, and the times of occurrence vary slightly.

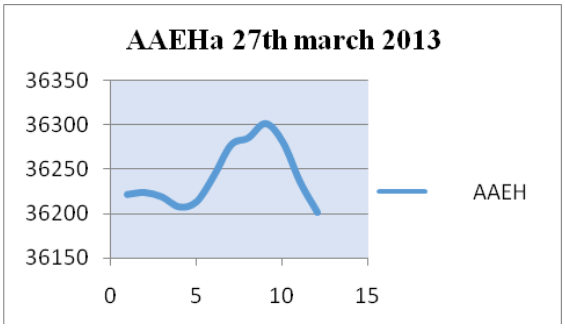

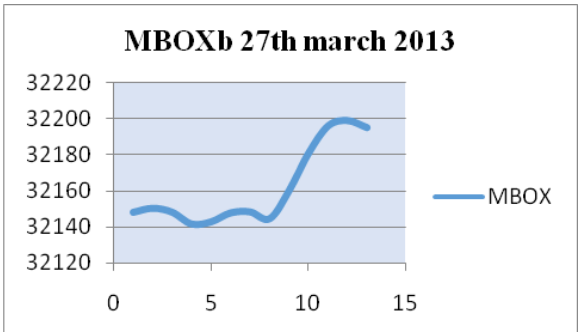

Fig 3.3a&b: Geomagnetic H&X-component against time (UT)

The strength of EEJ in Addis Ababa and Mbour is depicted in Figs. 3.3a and 3.3b, respectively. In Addis Ababa, the EEJ strength began to rise around 0800 UT and peaked at 1200 UT, whereas the strength of EEJ climbed between the hours of 0500 UT and began to decline about 0900 UT. No record was obtained at either station as of that time, according to the secret graph portion for the remainder hours of the day. The strength of EEJ during the hours of 0100 to 0900 UT was shown as a sinusoidal waveform in Fig. 3.3b.

IV. SUMMARY

Although they are located in the same coastal zone, Addis Ababa and Mbour experience varying EEJ intensities throughout time variations. As indicated in the above tables 3.1 and 3.2, Addis Ababa has a stronger EEJ than Mbour. Table 3.2 shows that the MBOY was negative, indicating that the Earth's southern hemisphere was where the Y-component of the geomagnetic field was detected. The abrupt drop and rise in EEJ strength at that specific moment, which may have been a result of several disturbance sources, was observed in Fig. 3.1a as an anomaly. It is evident from attentively examining each graph that the EEJ strength varied between the two stations. The degree of variability for both Addis Ababa and Mbour is indicated by the EEJ graph slope. The strength of EEJ from the geomagnetic field at Addis Ababa and Mbour is compared in this paper. Over time, the average strength of EEJ changes. The presented graph's slope indicates the level of variability and the impact of disturbances on the EEJ over time. The two survey stations, Addis Ababa and Mbour, have shown that the EEJ's strength fluctuates,

demonstrating that the Earth's geomagnetic field's latitude, longitude, and coastline regions all experience constant variation.

CONCLUSION

Observing the graph on 27th January 2013, it is clear to comprehend that the effect of EEJ on the geomagnetic H and X at Addis Ababa and Mbour is inconsistent, while on 27th February 2013, it is apparent that the geomagnetic H and X at Addis Ababa and Mbour experienced almost the same effect across the region at various time intervals. Nevertheless, on the 27th March 2013, there was a different impartation of the EEJ on the geomagnetic H and X at Addis Ababa and Mbour at the same variation in time. It is empirical to conclude that the strength of EEJ varies with time.

REFERENCES

[1] Alex, S., and Mukherjee, S., (2001), "Local time dependence of the equatorial counter electrojet effect in a narrow longitudinal belt." Earth Planets Space, 53, 1151–1161.

[2] Briggs, B. H., (1984), "The variability of ionospheric dynamo currents. Atmosphere". Terr. Phys., 59, 497–509.

[3] Campbell, W. H., (1989), "The regular geomagnetic-field variations during quiet solar conditions, in Geomagnetism". vol. 3, edited by J. A. Jacobs, pp. 385–460, Academic, San Diego, Calif.

[4] Campbell, W. H., (1990), "Differences in geomagnetic Sq field representations due to variations in spherical harmonic analysis techniques". J. Geophysics. Res., 95(A12), 20,923–20,936.

[5] Ekwubiri E. C., Aiyohuyin O. E., 2026, "Evaluation of the Fourth-degree Polynomial Correlation between Rotational Angular Velocity of Eighty-four Spiral Barred Galaxies with Radius", Iconic Research and Engineering Journal Volume 9 Issue 9 March 2026 Page 603- 616. DOI: https://doi.org/10.64388/IREV9I9-1714886

[6] Ekwubiri, E.C., and Said R.S., (Ed), 2015; "Estimation of the Strength of EEJ from Solar Quiet Hours". Lambert Academic Publishing. ISBN 978-3-659-45652-7

[7] Fejer, B, (2010), "Lunar-dependent equatorial ionospheric electrodynamics effects during sudden stratospheric warming".

[8] Forbes, J. M. (1981); "The Equatorial Electrojet, Rev. Geophysics". Space Phys., 19, 469–504.

[9] Hargreaves, J.K., (1992), "The solar-terrestrial environment," Cambridge Atmospheric and Space Sciences series, Cambridge Univ. Press, Cambridge, UK,

[10] Jursa, Adolph S., (1985), "Handbook of Geophysics and the Space Environment" Air Force Geophysics Lab, Hanscom AFB, MA.

[11] Kelly, M. C., (1989), "The Earth's Ionosphere", Academic Press, Inc., San Diego.

[12] Kivelson, M. G., and Russell C., (1995), "Introduction to Space Physics", Cambridge Univ. Press.

[13] Ratcliffe J.A, (1972), "An introduction to the ionosphere and magnetosphere". Cambridge University Press (UK).